optica

Cavity electro-optics in thin-film lithium niobate for efficient microwave-to-optical transduction

Jeffrey Holzgrafe,[1] Neil Sinclair,[1,2] Di Zhu,[1,3] Amirhassan Shams-Ansari,[1] Marco Colangelo,[3] Yaowen Hu,[1,4] Mian Zhang,[1,5] Karl K. Berggren,[3] and Marko Lončar[1,*]

[1]John A. Paulson School of Engineering and Applied Sciences, Harvard University, 29 Oxford Street, Cambridge, Massachusetts 02138, USA
[2]Division of Physics, Mathematics and Astronomy, and Alliance for Quantum Technologies, California Institute of Technology, 1200 E. California Boulevard, Pasadena, California 91125, USA
[3]Research Laboratory of Electronics, Massachusetts Institute of Technology, 50 Vassar Street, Cambridge, Massachusetts 02139, USA
[4]Department of Physics, Harvard University, 17 Oxford Street, Cambridge, Massachusetts 02138, USA
[5]HyperLight Corporation, 501 Massachusetts Avenue, Cambridge, Massachusetts 02139, USA
*Corresponding author: loncar@seas.harvard.edu

Received 12 May 2020; revised 20 September 2020; accepted 10 November 2020 (Doc. ID 397513); published 7 December 2020

Linking superconducting quantum devices to optical fibers via microwave-optical quantum transducers may enable large-scale quantum networks. For this application, transducers based on the Pockels electro-optic (EO) effect are promising for their direct conversion mechanism, high bandwidth, and potential for low-noise operation. However, previously demonstrated EO transducers require large optical pump power to overcome weak EO coupling and reach high efficiency. Here, we create an EO transducer in thin-film lithium niobate, a platform that provides low optical loss and strong EO coupling. We demonstrate on-chip transduction efficiencies of up to $(2.7 \pm 0.3) \times 10^{-5}$ and $(1.9 \pm 0.4) \times 10^{-6}/\mu W$ of optical pump power. The transduction efficiency can be improved by further reducing the microwave resonator's piezoelectric coupling to acoustic modes, increasing the optical resonator quality factor to previously demonstrated levels, and changing the electrode geometry for enhanced EO coupling. We expect that with further development, EO transducers in thin-film lithium niobate can achieve near-unity efficiency with low optical pump power.

https://doi.org/10.1364/OPTICA.397513

1. INTRODUCTION

Recent advances in superconducting quantum technology [1] have created interest in connecting these devices and systems into larger networks. Such a network can be built from relatively simple quantum interconnects [2] based on direct transmission of the few-photon microwave signals used in superconducting quantum devices [3]. However, the practical range of this approach is limited by the strong attenuation and thermal noise that microwave fields experience at room temperature. Therefore, quantum interconnects based on optical links have been explored as an alternative, because they provide long attenuation lengths, negligible thermal noise, and high bandwidth [4]. Connecting optical networks with superconducting quantum technologies requires a quantum transducer capable of converting single photons between microwave and optical frequencies [5,6]. Such a transducer offers a promising route toward both large-scale distributed superconducting quantum networks [7] and the scaling of superconductor quantum processors beyond single cryogenic environments [8,9]. Furthermore, single-photon microwave-to-optical transduction can be used to create high-efficiency modulators [10], detectors for individual microwave photons [11], and multiplexed readout of cryogenic electronics [12].

An ideal quantum transducer performs a unitary transformation on microwave and optical modes. Practically, this level of performance implies efficiency approaching 100%, low noise, and enough bandwidth for the desired signals [13]. Some of the most promising approaches toward quantum transduction have used electro- or piezo-optomechanical devices [14–25], nonlinear crystals that display a Pockels electro-optic (EO) effect [26–31], trapped atoms [32,33], crystals doped with rare-earth ions [34,35], and optomagnonic devices [36]. Although near-unitary performance has proved challenging to realize, the optomechanical approach (the leading platform to date) has been used to demonstrate bidirectional operation [14], high efficiency [15,22], and noise levels below a single photon [23,37]. Optomechanical devices provide strong interactions with both microwave and optical fields, but their reliance on an intermediate mechanical mode in the transduction process creates several challenges for near-unitary operation. The low-frequency (megahertz) mechanical modes used in membrane electro-optomechanical transducers [14,15] result in strong thermal noise even at temperatures below 100 mK,

and make the transducers susceptible to low-frequency technical noise sources. Although piezo-optomechanical devices that use gigahertz frequency mechanical modes [16–25] are not susceptible to these issues, such devices display optical-pump-induced heating of the mechanical resonator that adds to the transduction noise. This heating is difficult to avoid in piezo-optomechanical devices due to their colocalization of optical and mechanical modes, as well as their suspended nature that leads to high thermal resistance [38]. Pump-induced heating can be addressed using pulsed-pump schemes [39], but this approach requires trade-offs among efficiency, noise, and repetition rate [23,37].

The desire for lower noise, higher efficiency, and faster repetition rates has motivated research into cavity-based EO transducers [26–30,40–43], in which microwave fields directly modulate light using an EO nonlinearity of the host material. This approach has two main benefits. First, the direct conversion mechanism avoids any intermediate stages, reducing device complexity and eliminating some sources of loss and noise. Second, these devices can have spatially separated microwave and optical resonators with low thermal resistance to base temperature, potentially offering much lower optically induced thermal noise than suspended devices based on colocalized optical and mechanical modes. Previous EO transducers have used bulk lithium niobate [26–28], aluminum nitride [30], and hybrid silicon–organic [43] platforms. Recent work on EO transducers has shown promise for low-noise operation due to the efficient cooling of microwave modes in these systems [44–46]. To date, EO transducers have demonstrated bidirectional operation and on-chip efficiency as high as 2% for a relatively large ∼10 mW optical pump [30], yet power-normalized efficiencies remain low and would require large (∼1 W) optical pump powers to reach near-unity efficiency. The efficiency of EO transducers can be improved by minimizing the loss rates of the resonators and enhancing the EO interaction strength. Toward this end, here we use a thin-film lithium niobate platform, which combines a large EO coefficient of 32 pm/V, tight confinement of the optical mode to enable a strong EO coupling [47], and the ability to realize low-loss optical resonators with demonstrated quality factors (Q) of 10^7 [48]. These properties make lithium niobate a compelling platform for improving transduction efficiency with EO transducers.

Specifically, we describe an EO transducer made from a thin-film lithium niobate photonic molecule [49,50] integrated with a superconducting microwave resonator and demonstrate an on-chip transduction efficiency of greater than $10^{-6}/\mu$W of optical pump power for continuous-wave signals.

Despite the promising properties of the thin-film lithium niobate platform, this power-normalized efficiency is comparable to that achieved in previous EO transducers [28,30,44]. This is due partly to parasitic piezoelectric coupling that causes excess microwave resonator loss. Our transducer is designed to reduce this coupling, but doing so requires a sub-optimal electrode layout and still yields a relatively low microwave $Q \sim 10^3$. However, we show that with straightforward improvements—including better acoustic engineering—the efficiency can be increased to near unity for ∼100 μW of optical pump power. Outside its potential for high transduction efficiency and low noise, our platform has several other advantages for making a practical microwave-optical transducer. First, the small footprint (∼1 mm^2) compared to bulk EO transducers enables multiplexed designs for high-rate quantum communication [8,9]. Second, the triple-resonance photonic-molecule design of our device makes it easy to design for a particular transduction frequency. Finally, low-loss tunable filters can be integrated on-chip with our device to reduce filtering losses in transduction protocols [51].

2. DEVICE DESIGN AND CHARACTERIZATION

The operating principle of our transducer is illustrated in Fig. 1(a). Two lithium niobate optical ring resonators are evanescently coupled to create a pair of hybrid photonic-molecule modes, with a strong optical pump signal tuned to the red optical mode at ω_-. A superconducting microwave resonator with resonance frequency ω_m modulates the optical pump signal, upconverting photons from the microwave resonator to the blue optical mode at ω_+.

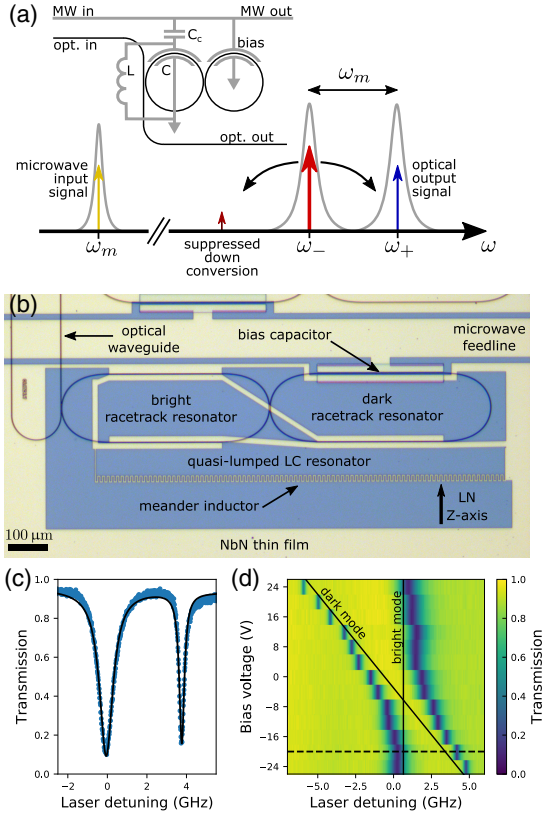

Fig. 1. Superconducting cavity electro-optic transducer on thin-film lithium niobate. (a) Top: device schematic. Black and gray lines represent optical waveguides and superconducting wires, respectively. The coupled optical ring resonators are modulated by a microwave (MW) resonator (made from inductor L and capacitor C) that is capacitively coupled to the bus (C_c). The optical resonance frequencies can be tuned by a bias capacitor. Bottom: frequency-domain diagram of the transduction scheme. A pump laser is tuned into resonance with the red optical mode at ω_-. Photons in the microwave resonator at ω_m can be upconverted to the blue optical mode at ω_+ by sum-frequency generation. (b) Optical micrograph of the transducer, showing optical waveguides (black) and the niobium nitride superconducting film (light yellow). The capacitor of the quasi-lumped LC resonator modulates the optical racetrack resonators. A DC voltage on the microwave feedline controls the detuning between optical modes. (c) Optical transmission spectrum near 1586 nm of a pair of photonic-molecule optical modes with a −20 V bias. (d) Optical transmission spectra at other bias voltages display an anticrossing between modes in the bright and dark racetrack resonators. Dashed line shows data in (c).

This transduction process is phase-coherent and can be described by a beam splitter interaction Hamiltonian:

$$H_I = \hbar g_0 \sqrt{n_-}\left(b^\dagger a_+ + b a_+^\dagger\right), \tag{1}$$

where g_0 is the single-photon EO interaction strength, n_- is the number of (pump) photons in the red optical mode, while b and a_+ are the annihilation operators for the microwave and blue optical modes, respectively. The interaction strength g_0 is determined by the microwave resonator's total capacitance, the overlap between microwave and optical modes, as well as the EO coefficient of the host material. We use a thin-film superconducting LC resonator and an integrated lithium niobate racetrack resonator [47] to optimize this interaction strength, which we estimate to be $g_0 = 2\pi \times 850$ Hz. The on-chip transduction efficiency η for continuous-wave signals depends on both this interaction strength and the loss rates of the modes (see Supplement 1, Section 1):

$$\eta = \frac{\kappa_{m,\mathrm{ex}}\kappa_{+,\mathrm{ex}}}{\kappa_m \kappa_+} \times \frac{4C}{(1+C)^2}, \tag{2}$$

where $(\kappa_{m,\mathrm{ex}}, \kappa_m)$ and $(\kappa_{+,\mathrm{ex}}, \kappa_+)$ are the external and total loss rates for the microwave and blue optical modes, respectively, and $C = \frac{4g_0^2 n_-}{\kappa_m \kappa_+}$ is the cooperativity. The first term in Eq. (2) represents the efficiency of a photon entering and exiting the transducer. To maximize this photon coupling efficiency, the resonators in our device are overcoupled.

A microscope image of our device is shown in Fig. 1(b). Light with TE polarization is coupled from an optical fiber array onto the chip using grating couplers with ≈ 10 dB insertion loss. The photonic-molecule optical modes are created using evanescently coupled racetrack resonators made from 1.2 μm wide rib waveguides in thin-film lithium niobate atop a 4.7 μm thick amorphous silicon dioxide layer on a silicon substrate. The optical waveguides are cladded with a 1.5 μm thick layer of amorphous silicon dioxide. The fabrication process for these optical resonators is described in detail in Ref. [49]. To create the superconducting resonator, a ≈ 40 nm thick niobium nitride film is deposited on top of the cladding by DC magnetron sputtering [52] and patterned using photolithography followed by CF_4 reactive ion etching. The detuning between the optical modes can be controlled using a bias capacitor on the dark (i.e., not directly coupled to the bus waveguide) racetrack resonator.

The optical transmission spectrum displayed in Fig. 1(c) shows a typical pair of quasi-TE photonic-molecule optical modes. As shown in Fig. 1(d), we observe a clear anticrossing between bright and dark resonator modes when tuning the bias voltage and measure a minimum optical mode splitting of 3.1 GHz. By measuring the resonance linewidths as a function of bias voltage [see Eq. (S4) in Supplement 1, Section 1], we infer that the unhybridized bright and dark optical modes have internal loss rates of $\kappa_{\mathrm{bright,in}} = 2\pi \times 350$ MHz and $\kappa_{\mathrm{dark,in}} = 2\pi \times 150$ MHz, respectively, and that the bright mode has an external loss rate of $\kappa_{\mathrm{bright,ex}} = 670$ MHz. In this work, we use several pairs of optical modes for microwave to optical transduction measurements. To understand the variability of optical loss across resonances in our device, we performed similar measurements on quasi-TE resonances between 1584–1593 nm and found the mean and standard deviation of the loss rates to be $\kappa_{\mathrm{bright,in}} = 2\pi \times (170 \pm 70)$ MHz, $\kappa_{\mathrm{dark,in}} = 2\pi \times (200 \pm 60)$ MHz, and $\kappa_{\mathrm{bright,ex}} = (830 \pm 300)$ MHz. These results correspond to an average internal quality factor of $Q_i \approx 10^6$.

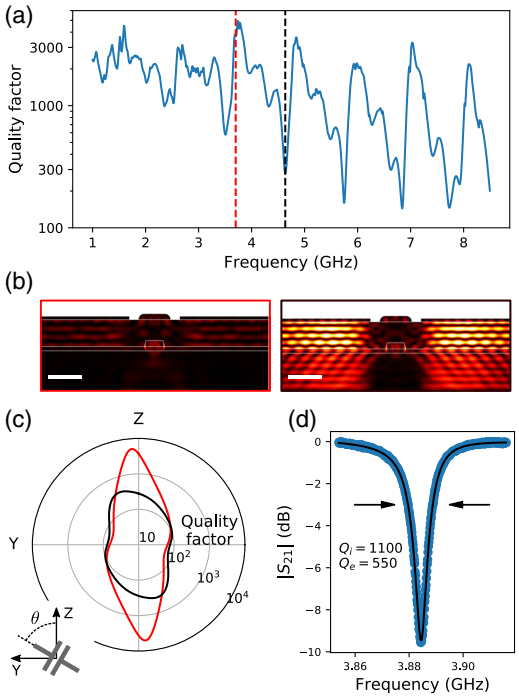

Fig. 2. Piezoelectric loss in lithium niobate. (a) Frequency dependence of the simulated microwave resonance loss caused by piezoelectric coupling to acoustic modes. Frequencies near bulk acoustic wave modes (e.g., black dashed line at 4.6 GHz) display strong loss, but relatively low-loss performance can be achieved for frequencies far detuned from bulk acoustic modes (e.g., red dashed line at 3.7 GHz). (b) Simulated acoustic energy density profiles of the device cross section for 3.7 GHz (red border) and 4.6 GHz (black border). White scale bars are 2 μm long. (c) Simulated microwave quality factor for different orientations of the capacitor with respect to the crystal axes of lithium niobate, at 3.7 GHz (red) and 4.6 GHz (black). (d) Measured microwave transmission spectrum of the microwave resonator at a temperature $T = 1$ K.

Lithium niobate has a strong piezoelectric susceptibility, which gives the microwave resonator a loss channel to traveling acoustic modes [53]. To investigate this loss mechanism, we perform a two-dimensional simulation of a cross section of the waveguide and resonator capacitor (see Supplement 1, Section 2). The simulated intrinsic microwave quality factor due to piezoelectric loss displays a strong frequency dependence, as shown in Fig. 2(a). This frequency dependence is caused by low-quality-factor bulk acoustic modes—illustrated in Fig. 2(b)—that form in the thin-film layers of our device, which resonantly enhance the coupling between the microwave resonator and acoustic fields. Lower loss can be achieved by designing the microwave resonance frequency to avoid the bulk acoustic resonances. The relative orientation of the capacitor and the lithium niobate crystal axes also influences the microwave loss. Figure 2(c) shows that the intrinsic microwave quality factor is maximized when the electric field produced by the capacitor is oriented close to the z axis of the lithium niobate crystal, which is also the condition that maximizes EO response. Using these considerations, we designed a microwave resonator that has a measured intrinsic quality factor of $Q_i = 1100$ at a temperature of 1 K, as shown in Fig. 2(d). In addition to piezoelectric effects, we also estimate that dielectric loss in the amorphous silicon

dioxide cladding contributes an added loss of $Q_{clad} \sim 2000$ to the resonator (see Supplement 1, Section 2). This dielectric loss can be reduced by changing the electrode design to minimize the participation fraction of the amorphous cladding, or using lower-loss cladding materials [54].

3. MICROWAVE-TO-OPTICAL TRANSDUCTION

To measure the transduction efficiency of our device, we locked the frequency of the pump to be near-resonant with the red optical mode (side-of-fringe locking) and sent a resonant microwave signal into the device. The pump and upconverted optical signals were collected and sent to an amplified photodetector, which produced a beat note at the input microwave frequency. We inferred the on-chip transduction efficiency from this beat note power by calibrating the input optical power, system losses, and detector efficiency (see Supplement 1, Section 3). During this transduction efficiency measurement, we swept the bias voltage in a triangle waveform with a period of ≈ 1 min to vary the splitting between the optical modes. The pump light remained locked to the red optical mode throughout the measurement. Figure 3(a) illustrates the optical modes and signals over the course of the bias voltage sweep.

The results of this measurement are depicted in Fig. 3. The two maxima in transduction efficiency near ± 10 V [Figs. 3(b) and 3(c)] correspond to the cases where the triple-resonance condition is met and the upconverted light is resonant with the blue optical mode. The shape of the optical anticrossing ensures this triple-resonance condition is met twice in the voltage sweep. For large negative bias voltages, the blue mode is far-detuned, and most of the upconverted light is generated in the red optical mode by a double-resonance process involving just the red optical mode and the microwave mode (see Supplement 1, Section 1C). This process does not depend on the resonance frequency of the blue optical mode, so the transduction efficiency is nearly independent of the bias voltage in this regime. Destructive interference of upconverted light produced in the red and blue optical modes (created by double- and triple-resonance processes, respectively) causes the transduction efficiency minimum near -20 V. For large positive bias voltage, the red optical mode is undercoupled and has a narrow linewidth, so the double-resonance transduction process is weak. The measured data presented in Fig. 3(c) show good correspondence to our analytical model shown in Fig. 3(b) [Eq. (S21) in Supplement 1, Section 1], which is based on independently measured and estimated device parameters.

As shown in Fig. 3(d), the frequency of the optical modes displays hysteresis when changing the bias voltage, which also causes the efficiency hysteresis in Fig. 3(c) We observed that this hysteresis could be reduced by lowering the optical pump power and sweeping the voltage bias faster. Based on the slow timescale (seconds for -30 dBm on-chip optical pump power), we attribute the hysteresis to photoconductive and photorefractive effects in lithium niobate [55]. These effects are caused by optical excitation of charge carriers from defects in the lithium niobate waveguide. These carriers migrate and create built-in electric fields that shift the optical resonance frequencies through the EO effect. Such photorefractive and photoconductive effects are known to be stronger and to operate at faster timescales in thin-film lithium niobate than in bulk devices [56,57]. In practice, these effects can be overcome by using pulsed-pump schemes to reduce carrier generation (see high power measurements below), modulating the bias voltage to prevent complete shielding of the bias field, and locking the laser to the optical resonances. We plan to study the impact of photoconductive and photorefractive effects on the low-frequency EO response of thin-film lithium niobate devices in future work.

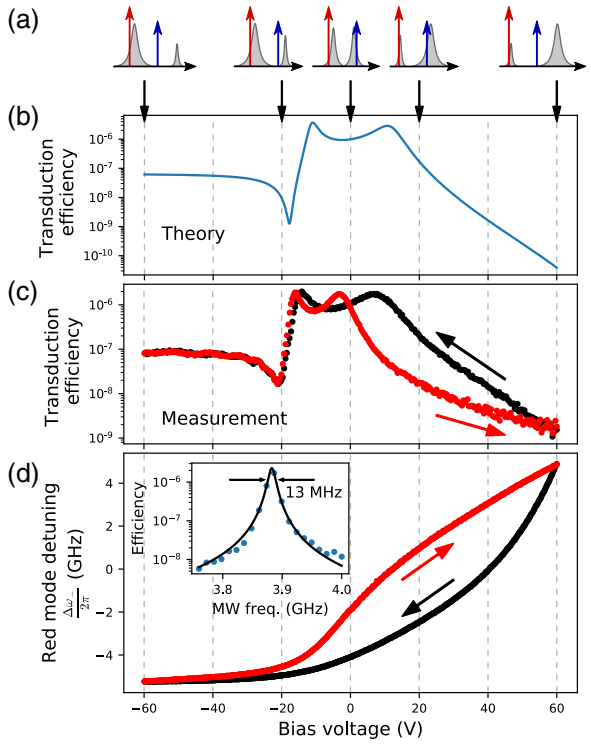

Fig. 3. Detuning dependence of microwave-to-optical photon transduction. (a) Frequency-domain illustrations of the optical modes for the bias voltages indicated by the downward-facing arrows. (b) Predicted dependence of the on-chip transduction efficiency on the bias voltage. This prediction is based on a model that includes transduction into both the red and blue optical modes, and independently measured and calculated device parameters. (c) Measured dependence of the on-chip transduction efficiency on the bias voltage. Red and black traces correspond to sweeps of increasing and decreasing voltage, respectively. (d) Red optical mode frequency detuning induced by the bias voltage during the transduction experiment. Inset: the dependence of the highest on-chip transduction efficiency on the frequency of the microwave drive displays a wide bandwidth of 13 MHz. All data shown for -30 dBm on-chip optical pump power.

We measured the bandwidth of the transducer by varying the frequency of the input microwave drive and measuring the highest transduction efficiency reached during a bias voltage sweep. The inset of Fig. 3(d) shows that our transducer has a 3 dB bandwidth of 13 MHz, slightly larger than the measured 10 MHz linewidth of the microwave resonator. This discrepancy is caused by the nonlinear response of the NbN microwave resonator for high microwave power, which leads to an apparent resonance broadening [58] (see Supplement 1, Section 4). To reduce measurement noise, here we use a relatively large microwave power (-38 dBm on-chip), which causes a small degree of nonlinear broadening. This nonlinearity also leads to reduced transduction efficiency for large-input microwave powers [Fig. 4(a) inset].

Figure 4(a) shows the highest on-chip transduction efficiency measured during a bias voltage sweep for different optical pump powers. During this measurement, we found that the zero-bias detuning between the optical modes could change by several

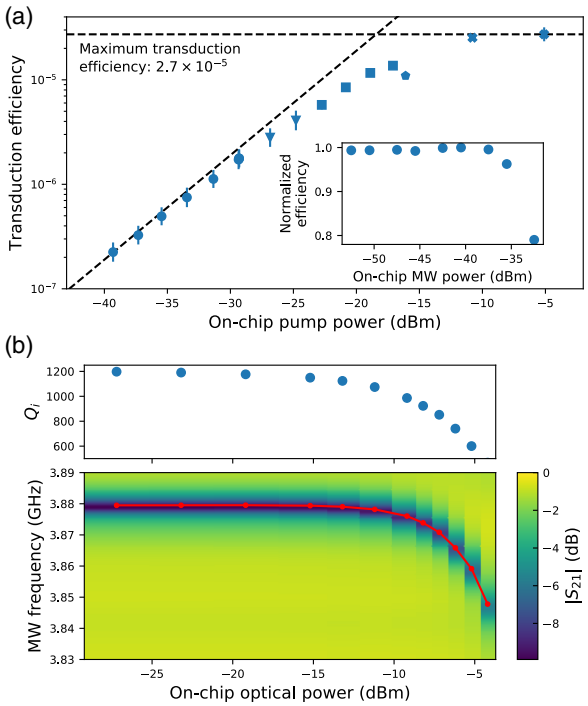

Fig. 4. Power dependence of microwave-to-optical photon transduction. (a) Maximum on-chip transduction efficiency measured during a sweep of the bias voltage for different optical pump powers. The different markers (circles, triangles, etc.) correspond to sets of measurements performed on different optical modes (see main text for details). Inset: dependence of the transduction efficiency on microwave input power for −30 dBm on-chip optical pump power. (b) Degradation of the microwave resonator due to absorption of pump light. The plots show the optical power dependence of the microwave transmission spectrum (bottom, red line denotes resonance frequency) and the inferred intrinsic microwave quality factor (top).

gigahertz when the optical pump power was varied, due likely to the photoconductive and photorefractive effects described earlier. To measure the transduction efficiency at the triple-resonance point for each power level, we performed measurements on several pairs of photonic-molecule modes. For the highest optical pump powers used in this study [denoted by crosses in Fig. 4(a)], we modulated the optical pump to extinction at a rate of 20 kHz and with a 10% duty cycle. The lower average power in these modulated-pump measurements resulted in smaller power-dependent detunings and more stable resonances.

In the low-power regime (< -30 dBm), we observe that the transduction efficiency scales linearly with pump power at a rate of $(1.9 \pm 0.4) \times 10^{-6}/\mu$W. From this and the measured loss rates of the resonators, we estimate the single-photon coupling rate of our transducer to be $g_0 = 2\pi \times 650 \pm 80$ Hz, comparable in magnitude to the predicted $g_0 = 2\pi \times 850$ Hz (see Supplement 1, Section 1D), yet slightly lower than expected. This difference is due likely to variations in the as-fabricated geometry of the device.

The on-chip transduction efficiency begins to saturate at $(2.7 \pm 0.3) \times 10^{-5}$, the highest-measured efficiency for this transducer. This saturation is caused by optical absorption in the microwave resonator, which generates quasiparticles that shift the resonance frequency and increase the loss rate of the resonator [59]. Figure 4(b) shows the optical-power dependence of the microwave resonator's properties. We find that the quasiparticle-induced changes in the microwave resonator are independent of whether the pump laser is tuned on- or off-resonance with an optical mode, which suggests that the absorbed light does not come from the optical resonator itself. Instead, stray light scattered at the fiber array and grating couplers is the dominant contribution to the quasiparticle loss.

Note that although we did not demonstrate optical-to-microwave transduction (only microwave-to-optical) due to a low signal-to-noise ratio, the EO transduction process is fully bidirectional (see Supplement 1, Section 1).

4. DISCUSSION AND CONCLUSION

The transduction efficiency demonstrated here falls well below the requirements for a useful quantum transducer. However, the straightforward changes to the transducer shown in Table 1 can greatly improve this figure of merit. First, optical quality factors above 10^7 have been demonstrated in thin-film lithium niobate [48], suggesting that the optical loss rates seen here can be reduced by roughly 10-fold, leading to a 100-fold improvement in transduction efficiency. Second, the microwave resonator loss rate can be reduced through improved engineering of the bulk acoustic waves to which the microwave resonator couples and elimination of amorphous cladding materials. For example, simulations suggest that suspending the lithium niobate layer can reduce the microwave loss by more than 10-fold. Third, the optically induced quasiparticle losses can be greatly reduced by changing the design of the sample mount and optical fiber coupling to shield the microwave resonator from stray scattered light. By implementing these and other smaller changes (see Table 1 and Supplement 1, Section 5 for details), we predict that near-unity transduction efficiency can be achieved for optical pump powers of ∼100 μW.

In this work, we have demonstrated transduction between microwave and optical frequencies using a thin-film lithium niobate device. The photonic-molecule design of our transducer

Table 1. Predicted Improvements in Device Parameters

Parameter	Improvement Factor	Efficiency Enhancement	Notes
$\kappa_{optical}$	10	10^2	Optical quality factor $Q = 10^7$
κ_m	10	10	By suspending lithium niobate layer
Block scattered light	—	10	For 100 μW of on-chip pump power
Electrode coverage	2	4	
Single-sided MW coupling	2	2	Improves effective MW loss
Microwave capacitance	2	1.5	Using a high-impedance inductor
Resonant optical pump	—	1.5	
Total		∼10^5	

enables straightforward tuning of the optical modes using a bias voltage, ensures strong suppression of the downconverted light that acts as a noise source, and takes full advantage of the large EO coefficient in lithium niobate. We have described how the piezoelectric coupling of the microwave resonator to traveling acoustic waves can be engineered to minimize loss in the microwave resonator. The advantages of an EO transducer—namely, the system simplicity, promise for low-noise operation, and possibility for on-chip filter integration—and the opportunities for improved transduction efficiency motivate further development of thin-film lithium niobate cavity electro-optics.

Note. During the preparation of this paper, we became aware of a similar lithium niobate quantum transducer device reported by McKenna *et al.* [60].

Funding. Office of Naval Research (N00014-15-1-2761); U.S. Department of Energy (DE-SC0019219); Natural Sciences and Engineering Research Council of Canada; AQT Intelligent Quantum Networks and Technologies; National Science Foundation (ECCS-1541959, ECCS-1839197, NSF 1541959).

Acknowledgment. This work was performed in part at the Center for Nanoscale Systems (CNS), a member of the National Nanotechnology Coordinated Infrastructure Network (NNCI), which is supported by the National Science Foundation. CNS is part of Harvard University. D.Z. is supported by the Harvard Quantum Initiative (HQI) postdoctoral fellowship. The authors thank C.J. Xin, E. Puma, B. Machielse, C. Wang, Y. Qiu, and W. Oliver for helpful discussions and assistance with device fabrication.

Disclosures. MZ: HyperLight Corporation (I,E). ML: Hyperlight Corporation (I,S).

See Supplement 1 for supporting content.

REFERENCES

1. G. Wendin, "Quantum information processing with superconducting circuits: a review," Rep. Prog. Phys. **80**, 106001 (2017).
2. D. Awschalom, K. K. Berggren, H. Bernien, S. Bhave, L. D. Carr, P. Davids, S. E. Economou, D. Englund, A. Faraon, M. Fejer, S. Guha, M. V. Gustafsson, E. Hu, L. Jiang, J. Kim, B. Korzh, P. Kumar, P. G. Kwiat, M. Lončar, M. D. Lukin, D. A. B. Miller, C. Monroe, S. W. Nam, P. Narang, J. S. Orcutt, M. G. Raymer, A. H. Safavi-Naeini, M. Spiropulu, K. Srinivasan, S. Sun, J. Vučković, E. Waks, R. Walsworth, A. M. Weiner, and Z. Zhang, "Development of quantum interconnects for next-generation information technologies," arXiv:1912.06642 [quant-ph] (2020).
3. P. Kurpiers, P. Magnard, T. Walter, B. Royer, M. Pechal, J. Heinsoo, Y. Salathé, A. Akin, S. Storz, J.-C. Besse, S. Gasparinetti, A. Blais, and A. Wallraff, "Deterministic quantum state transfer and remote entanglement using microwave photons," Nature **558**, 264–267 (2018).
4. J. L. O'Brien, A. Furusawa, and J. Vučković, "Photonic quantum technologies," Nat. Photonics **3**, 687–695 (2009).
5. N. J. Lambert, A. Rueda, F. Sedlmeir, and H. G. L. Schwefel, "Coherent conversion between microwave and optical photons—an overview of physical implementations," Adv. Quantum Technol. **3**, 1900077 (2020).
6. N. Lauk, N. Sinclair, S. Barzanjeh, J. P. Covey, M. Saffman, M. Spiropulu, and C. Simon, "Perspectives on quantum transduction," Quantum Sci. Technol. **5**, 020501 (2020).
7. S. Wehner, D. Elkouss, and R. Hanson, "Quantum internet: a vision for the road ahead," Science **362**, eaam9288 (2018).
8. N. H. Nickerson, J. F. Fitzsimons, and S. C. Benjamin, "Freely scalable quantum technologies using cells of 5-to-50 qubits with very lossy and noisy photonic links," Phys. Rev. X **4**, 041041 (2014).
9. C. Monroe, R. Raussendorf, A. Ruthven, K. R. Brown, P. Maunz, L.-M. Duan, and J. Kim, "Large scale modular quantum computer architecture with atomic memory and photonic interconnects," Phys. Rev. A **89**, 022317 (2014).
10. H. Gevorgyan, A. Khilo, Y. Ehrlichman, M. A. Popović, and M. A. Popović, "Triply resonant coupled-cavity electro-optic modulators for RF to optical signal conversion," Opt. Express **28**, 788–815 (2020).
11. T. Bagci, A. Simonsen, S. Schmid, L. G. Villanueva, E. Zeuthen, J. Appel, J. M. Taylor, A. Sørensen, K. Usami, A. Schliesser, and E. S. Polzik, "Optical detection of radio waves through a nanomechanical transducer," Nature **507**, 81–85 (2014).
12. M. de Cea, E. E. Wollman, A. H. Atabaki, D. J. Gray, M. D. Shaw, and R. J. Ram, "Photonic readout of superconducting nanowire single photon counting detectors," Sci. Rep. **10**, 9470 (2020).
13. E. Zeuthen, A. Schliesser, A. S. Sørensen, and J. M. Taylor, "Figures of merit for quantum transducers," Quantum Sci. Technol. **5**, 034009 (2020).
14. R. W. Andrews, R. W. Peterson, T. P. Purdy, K. Cicak, R. W. Simmonds, C. A. Regal, and K. W. Lehnert, "Bidirectional and efficient conversion between microwave and optical light," Nat. Phys. **10**, 321–326 (2014).
15. A. P. Higginbotham, P. S. Burns, M. D. Urmey, R. W. Peterson, N. S. Kampel, B. M. Brubaker, G. Smith, K. W. Lehnert, and C. A. Regal, "Harnessing electro-optic correlations in an efficient mechanical converter," Nat. Phys. **14**, 1038–1042 (2018).
16. L. Midolo, A. Schliesser, and A. Fiore, "Nano-opto-electro-mechanical systems," Nat. Nanotechnol. **13**, 11–18 (2018).
17. A. H. Safavi-Naeini, D. V. Thourhout, R. Baets, and R. V. Laer, "Controlling phonons and photons at the wavelength scale: integrated photonics meets integrated phononics," Optica **6**, 213–232 (2019).
18. J. Bochmann, A. Vainsencher, D. D. Awschalom, and A. N. Cleland, "Nanomechanical coupling between microwave and optical photons," Nat. Phys. **9**, 712–716 (2013).
19. L. Fan, X. Sun, C. Xiong, C. Schuck, and H. X. Tang, "Aluminum nitride piezo-acousto-photonic crystal nanocavity with high quality factors," Appl. Phys. Lett. **102**, 153507 (2013).
20. K. C. Balram, M. I. Davanço, J. D. Song, and K. Srinivasan, "Coherent coupling between radiofrequency, optical and acoustic waves in piezo-optomechanical circuits," Nat. Photonics **10**, 346–352 (2016).
21. A. Vainsencher, K. J. Satzinger, G. A. Peairs, and A. N. Cleland, "Bi-directional conversion between microwave and optical frequencies in a piezoelectric optomechanical device," Appl. Phys. Lett. **109**, 033107 (2016).
22. W. Jiang, C. J. Sarabalis, Y. D. Dahmani, R. N. Patel, F. M. Mayor, T. P. McKenna, R. Van Laer, and A. H. Safavi-Naeini, "Efficient bidirectional piezo-optomechanical transduction between microwave and optical frequency," Nat. Commun. **11**, 1166 (2020).
23. M. Forsch, R. Stockill, A. Wallucks, I. Marinković, C. Gärtner, R. A. Norte, F. van Otten, A. Fiore, K. Srinivasan, and S. Gröblacher, "Microwave-to-optics conversion using a mechanical oscillator in its quantum ground state," Nat. Phys. **16**, 69–74 (2020).
24. L. Shao, M. Yu, S. Maity, N. Sinclair, L. Zheng, C. Chia, A. Shams-Ansari, C. Wang, M. Zhang, K. Lai, and M. Lončar, "Microwave-to-optical conversion using lithium niobate thin-film acoustic resonators," Optica **6**, 1498–1505 (2019).
25. X. Han, W. Fu, C. Zhong, C.-L. Zou, Y. Xu, A. A. Sayem, M. Xu, S. Wang, R. Cheng, L. Jiang, and H. X. Tang, "Cavity piezo-mechanics for superconducting-nanophotonic quantum interface," Nat. Commun. **11**, 3237 (2020).
26. V. S. Ilchenko, A. A. Savchenkov, A. B. Matsko, and L. Maleki, "Whispering-gallery-mode electro-optic modulator and photonic microwave receiver," J. Opt. Soc. Am. B **20**, 333–342 (2003).
27. D. V. Strekalov, A. A. Savchenkov, A. B. Matsko, and N. Yu, "Efficient upconversion of subterahertz radiation in a high-Q whispering gallery resonator," Opt. Lett. **34**, 713–715 (2009).
28. A. Rueda, F. Sedlmeir, M. C. Collodo, U. Vogl, B. Stiller, G. Schunk, D. V. Strekalov, C. Marquardt, J. M. Fink, O. Painter, G. Leuchs, and H. G. L. Schwefel, "Efficient microwave to optical photon conversion: an electro-optical realization," Optica **3**, 597–604 (2016).
29. J. D. Witmer, J. A. Valery, P. Arrangoiz-Arriola, C. J. Sarabalis, J. T. Hill, and A. H. Safavi-Naeini, "High-Q photonic resonators and electro-optic coupling using silicon-on-lithium-niobate," Sci. Rep. **7**, 46313 (2017).

30. L. Fan, C.-L. Zou, R. Cheng, X. Guo, X. Han, Z. Gong, S. Wang, and H. X. Tang, "Superconducting cavity electro-optics: a platform for coherent photon conversion between superconducting and photonic circuits," Sci. Adv. **4**, eaar4994 (2018).
31. J. D. Witmer, T. P. McKenna, W. Jiang, P. Arrangoiz-Arriola, E. A. Wollack, R. Van Laer, and A. H. Safavi-Naeini, "On-chip microwave-to-optical photonconversion for quantum networks," in *Quantum Information and Measurement (QIM) V: Quantum Technologies*, (OSA, , 2019), paper T5A.10.
32. T. Vogt, C. Gross, J. Han, S. B. Pal, M. Lam, M. Kiffner, and W. Li, "Efficient microwave-to-optical conversion using Rydberg atoms," Phys. Rev. A **99**, 023832 (2019).
33. J. Han, T. Vogt, C. Gross, D. Jaksch, M. Kiffner, and W. Li, "Coherent microwave-to-optical conversion via six-wave mixing in Rydberg atoms," Phys. Rev. Lett. **120**, 093201 (2018).
34. X. Fernandez-Gonzalvo, Y.-H. Chen, C. Yin, S. Rogge, and J. J. Longdell, "Coherent frequency up-conversion of microwaves to the optical telecommunications band in an Er:YSO crystal," Phys. Rev. A **92**, 062313 (2015).
35. J. G. Bartholomew, J. Rochman, T. Xie, J. M. Kindem, A. Ruskuc, I. Craiciu, M. Lei, and A. Faraon, "On-chip coherent microwave-to-optical transduction mediated by ytterbium in YVO_4," Nat. Commun. **11**, 3266 (2020).
36. R. Hisatomi, A. Osada, Y. Tabuchi, T. Ishikawa, A. Noguchi, R. Yamazaki, K. Usami, and Y. Nakamura, "Bidirectional conversion between microwave and light via ferromagnetic magnons," Phys. Rev. B **93**, 174427 (2016).
37. M. Mirhosseini, A. Sipahigil, M. Kalaee, and O. Painter, "Quantum transduction of optical photons from a superconducting qubit," arXiv:2004.04838 [quant-ph] (2020).
38. S. M. Meenehan, J. D. Cohen, S. Gröblacher, J. T. Hill, A. H. Safavi-Naeini, M. Aspelmeyer, and O. Painter, "Silicon optomechanical crystal resonator at millikelvin temperatures," Phys. Rev. A **90**, 011803 (2014).
39. S. M. Meenehan, J. D. Cohen, G. S. MacCabe, F. Marsili, M. D. Shaw, and O. Painter, "Pulsed excitation dynamics of an optomechanical crystal resonator near its quantum ground state of motion," Phys. Rev. X **5**, 041002 (2015).
40. M. Tsang, "Cavity quantum electro-optics," Phys. Rev. A **81**, 063837 (2010).
41. M. Tsang, "Cavity quantum electro-optics. II. Input-output relations between traveling optical and microwave fields," Phys. Rev. A **84**, 043845 (2011).
42. C. Javerzac-Galy, K. Plekhanov, N. R. Bernier, L. D. Toth, A. K. Feofanov, and T. J. Kippenberg, "On-chip microwave-to-optical quantum coherent converter based on a superconducting resonator coupled to an electro-optic microresonator," Phys. Rev. A **94**, 053815 (2016).
43. J. D. Witmer, T. P. McKenna, P. Arrangoiz-Arriola, R. V. Laer, E. A. Wollack, F. Lin, A. K.-Y. Jen, J. Luo, and A. H. Safavi-Naeini, "A silicon-organic hybrid platform for quantum microwave-to-optical transduction," Quantum Sci. Technol. **5**, 034004 (2020).
44. W. Hease, A. Rueda, R. Sahu, M. Wulf, G. Arnold, H. G. L. Schwefel, and J. M. Fink, "Bidirectional electro-opticwavelength conversion in the quantum ground state," PRX Quantum **1**, 020315 (2020).
45. S. Mobassem, N. J. Lambert, A. Rueda, J. M. Fink, G. Leuchs, and H. G. L. Schwefel, "Thermal noise in electro-optic devices at cryogenic temperatures," arXiv:2008.08764 [physics, physics:quant-ph] (2020).
46. W. Fu, M. Xu, X. Liu, C.-L. Zou, C. Zhong, X. Han, M. Shen, Y. Xu, R. Cheng, S. Wang, L. Jiang, and H. X. Tang, "Ground-state pulsed cavity electro-optics for microwave-to-optical conversion," arXiv:2010.11392 [physics, physics:quant-ph] (2020).
47. C. Wang, M. Zhang, X. Chen, M. Bertrand, A. Shams-Ansari, S. Chandrasekhar, P. Winzer, and M. Lončar, "Integrated lithium niobate electro-optic modulators operating at CMOS-compatible voltages," Nature **562**, 101–104 (2018).
48. M. Zhang, C. Wang, R. Cheng, A. Shams-Ansari, and M. Lončar, "Monolithic ultra-high-Q lithium niobate microring resonator," Optica **4**, 1536–1537 (2017).
49. M. Zhang, C. Wang, Y. Hu, A. Shams-Ansari, T. Ren, S. Fan, and M. Lončar, "Electronically programmable photonic molecule," Nat. Photonics **13**, 36–40 (2019).
50. M. Soltani, M. Zhang, C. Ryan, G. J. Ribeill, C. Wang, and M. Loncar, "Efficient quantum microwave-to-optical conversion using electro-optic nanophotonic coupled resonators," Phys. Rev. A **96**, 043808 (2017).
51. C. Wang, M. Zhang, M. Yu, R. Zhu, H. Hu, and M. Loncar, "Monolithic lithium niobate photonic circuits for Kerr frequency comb generation and modulation," Nat. Commun. **10**, 978 (2019).
52. A. E. Dane, A. N. McCaughan, D. Zhu, Q. Zhao, C.-S. Kim, N. Calandri, A. Agarwal, F. Bellei, and K. K. Berggren, "Bias sputtered NbN and superconducting nanowire devices," Appl. Phys. Lett. **111**, 122601 (2017).
53. M. Scigliuzzo, L. E. Bruhat, A. Bengtsson, J. J. Burnett, A. F. Roudsari, and P. Delsing, "Phononic loss in superconducting resonators on piezoelectric substrates," New J. Phys. **22**, 053027 (2020).
54. A. D. O'Connell, M. Ansmann, R. C. Bialczak, M. Hofheinz, N. Katz, E. Lucero, C. McKenney, M. Neeley, H. Wang, E. M. Weig, A. N. Cleland, and J. M. Martinis, "Microwave dielectric loss at single photon energies and millikelvin temperatures," Appl. Phys. Lett. **92**, 112903 (2008).
55. P. Günter and J.-P. Huignard, eds., *Photorefractive Materials and Their Applications 1: Basic Effects*, Springer Series in Optical Sciences (Springer, 2006), Vol. **113**.
56. H. Jiang, R. Luo, H. Liang, X. Chen, Y. Chen, and Q. Lin, "Fast response of photorefraction in lithium niobate microresonators," Opt. Lett. **42**, 3267–3270 (2017).
57. M. Li, H. Liang, R. Luo, Y. He, J. Ling, and Q. Lin, "Photon-level tuning of photonic nanocavities," Optica **6**, 860–863 (2019).
58. B. Abdo, E. Segev, O. Shtempluck, and E. Buks, "Nonlinear dynamics in the resonance line shape of NbN superconducting resonators," Phys. Rev. B **73**, 134513 (2006).
59. J. Zmuidzinas, "Superconducting microresonators: physics and applications," Annu. Rev. Condens. Matter Phys. **3**, 169–214 (2012).
60. T. P. McKenna, J. D. Witmer, R. N. Patel, W. Jiang, R. Van Laer, P. Arrangoiz-Arriola, E. A. Wollack, J. F. Herrmann, and A. H. Safavi-Naeini, "Cryogenic microwave-to-optical conversion using a triply-resonant lithium niobate on sapphire transducer," Optica **7**, 1737–1745 (2020).